JGR Solid Earth

RESEARCH ARTICLE
10.1029/2023JB027514

Hematite Frictional Behavior and He Loss From Comminution During Deformation Experiments at Slow Slip Rates

A. A. DiMonte[1], A. K. Ault[1], G. Hirth[2], and C. D. Meyers[2]

[1]Department of Geosciences, Utah State University, Logan, UT, USA, [2]Department of Earth, Environmental and Planetary Sciences, Brown University, Providence, RI, USA

Key Points:

- We performed rotary-shear experiments on coarse-grained hematite rock slabs to assess frictional behavior and Helium loss at slow slip rates
- Hematite has a moderate to high coefficient of friction and is velocity strengthening to velocity neutral at slow slip rates
- Helium loss in gouge occurs in the absence of temperature rise by grain size reduction that exposes Helium along new grain boundaries

Supporting Information:

Supporting Information may be found in the online version of this article.

Correspondence to:

A. A. DiMonte,
alex.dimonte@usu.edu

Citation:

DiMonte, A. A., Ault, A. K., Hirth, G., & Meyers, C. D. (2024). Hematite frictional behavior and He loss from comminution during deformation experiments at slow slip rates. *Journal of Geophysical Research: Solid Earth*, *129*, e2023JB027514. https://doi.org/10.1029/2023JB027514

Received 24 JULY 2023
Accepted 29 FEB 2024

Author Contributions:

Conceptualization: A. A. DiMonte, A. K. Ault, G. Hirth
Formal analysis: A. A. DiMonte
Funding acquisition: A. K. Ault, G. Hirth
Investigation: A. A. DiMonte, C. D. Meyers
Methodology: A. A. DiMonte, A. K. Ault, C. D. Meyers
Project administration: A. K. Ault
Resources: A. K. Ault, G. Hirth
Supervision: A. K. Ault, G. Hirth, C. D. Meyers
Visualization: A. A. DiMonte
Writing – original draft: A. A. DiMonte
Writing – review & editing: A. A. DiMonte, A. K. Ault, G. Hirth

Abstract Deformation experiments on hematite characterize its slip-rate dependent frictional properties and deformation mechanisms. These data inform interpretations of slip behavior from exhumed hematite-coated faults and present-day deformation at depth. We used a rotary-shear apparatus to conduct single-velocity and velocity-step experiments on polycrystalline specular hematite rock (~17 μm average plate thickness) at slip rates of 0.85 μm/s to 320 mm/s, displacements of primarily 1–3 cm and up to 45 cm, and normal stresses of 5 and 8.5 MPa. The average coefficient of friction is 0.70; velocity-step experiments indicate velocity-strengthening to velocity-neutral behavior at rates <1 mm/s. Scanning electron microscopy showed experimentally generated faults develop in a semi-continuous, thin layer of red hematite gouge. Angular gouge particles have an average diameter of ~0.7 μm, and grain size reduction during slip yields a factor of 10–100 increase in surface area. Hematite is amenable to (U-Th)/He thermochronometry, which can quantify fault-related thermal and mechanical processes. Comparison of hematite (U-Th)/He dates from the undeformed material and experimentally produced gouge indicates He loss occurs during comminution at slow deformation rates without an associated temperature rise required for diffusive loss. Our results imply that, in natural fault rocks, deformation localizes within coarse-grained hematite by stable sliding, and that hematite (U-Th)/He dates acquired from ultracataclasite or highly comminuted gouge reflect minor He loss unrelated to thermal processes. Consequently, the magnitude of temperature rise and associated thermal resetting in hematite-bearing fault rocks based on (U-Th)/He thermochronometry may be overestimated if only diffusive loss of He is considered.

Plain Language Summary Laboratory deformation experiments on hematite, a common iron-oxide in the shallow portion of fault zones, characterize its frictional properties and how it deforms in natural fault systems. We conducted experiments on bare surfaces of hematite rock at dominantly low sliding velocity, cm-scale displacements, and low normal stresses. Experiments showed that, at these conditions, hematite has a friction coefficient similar to many common rocks and minerals. In experiments where slip velocity is varied, hematite strengthens or retains the same strength with increasing slip rate. High spatial resolution microscopy showed experimental faults localize in a thin layer of hematite particles created from grain size reduction during slip. Radiometric dating of hematite via (U-Th)/He thermochronometry constrains the time when He, a noble gas, is trapped in a crystal, although both thermal or mechanical perturbations can cause He loss. Comparison of hematite (U-Th)/He dates from the undeformed rock and particles generated during laboratory slip indicates He was lost along newly generated particle surfaces during grain size reduction at slip rates <1 mm/s. Our results imply hematite deforms brittlely in nature at subseismic slip rates in shallow crustal conditions. (U-Th)/He dates acquired from natural, comminuted hematite may reflect some He loss unrelated to thermal processes.

1. Introduction

Fault composition evolves as a fault matures, (e.g., Janecke & Evans, 1988; Williams et al., 2021; Wintsch et al., 1995) and investigating the frictional behavior of minerals that form within fault zones over time provides insight into fault mechanics and modes of slip. Observations from natural fault rocks can be paired with laboratory experiments to constrain rate-and-state frictional behavior (Dieterich, 1979; Ruina, 1983) and potential deformation mechanisms (e.g., De Paola et al., 2015; Pozzi et al., 2018) in minerals and rocks at depth today. For example, aseismic creep is thought to occur on weak faults with a phyllosilicate-rich mineralogy that promotes velocity-strengthening behavior and stable sliding (Behnsen & Faulkner, 2012; Carpenter et al., 2012; Colletini et al., 2009; Kaduri et al., 2017; Moore et al., 2016; Moore & Lockner, 2004; Morrow et al., 1992, 2000; Reinen

et al., 1991; Saffer & Marone, 2003; Schleicher et al., 2010). Strong materials that adhere to Byerlee's law and weaken with increasing rate are velocity-weakening and promote unstable behavior if the fault stress or velocity reach a critical value (Gu et al., 1984; Leeman et al., 2016; Marone, 1998; Scholz, 2019).

Hematite is a common mineral in fault zones. Iron (Fe) is the fourth-most common element in the Earth, and hematite is a secondary mineral that precipitates from Fe-rich fluids present in or migrating through shallow fractures or fault zones, or from alteration of Fe-bearing host rock (Allegre et al., 1995; Ault, 2020; Cornell & Schwertmann, 2003). Hematite textures and grain morphologies along natural fault surfaces reflect the initial precipitation conditions and post-formation thermal, chemical, and mechanical processes (Ault, 2020). Integration of textural observations with hematite (U-Th)/He (hematite He) thermochronometry can inform the timing, temperatures, depths, and rates of fault slip (Ault, 2020). For example, hematite fault mirrors comprise ultracataclasite with regions of euhedral, "polygonal" grain morphologies at the slip interface, reflecting localized, transient amorphization and subsequent grain growth or rapid dynamic recrystallization that accompany high temperatures during seismic slip (Ault et al., 2015, 2019; McDermott et al., 2017, 2023; Odlum et al., 2022). Coseismic temperature rise induces He loss in hematite via recrystallization or thermally activated volume diffusion, resulting in hematite He dates that postdate hematite formation (Ault et al., 2015; McDermott et al., 2017). Other hematite fault surfaces, composed of nanometer-scale, foliated hematite platelets, develop and deform at subseismic slip rates, and most hematite He dates from such fault zones are interpreted to record the timing of the initial hematite formation (DiMonte et al., 2022; McDermott et al., 2021; Moser et al., 2017). Documenting the frictional behavior of hematite and textures that form over a range of slip rates and displacements in the lab is critical for refining these interpretations of slip rate and behavior, as well as (U-Th)/He dates in nature.

Prior work characterized frictional properties and He loss from coarse-grained, intact, specular hematite using an Instron rotary-shear apparatus (Calzolari et al., 2020). Hematite was deformed by slide-hold-slide (or "interrupted slip") and "continuous slip" experiments conducted at rates up to ~320 mm/s, 1.5 m of displacement, and 8.5 MPa normal stress (Calzolari et al., 2020). In these experiments, hematite exhibits subtle dynamic weakening behavior (i.e., a drop to a lower coefficient of friction following ~2 mm of slip at 320 mm/s, Di Toro et al., 2004; Di Toro et al., 2011). Recalibration of the torque cell on the Instron indicates the coefficient of friction (μ) reported from these prior experiments was underestimated; the previously reported value of 0.28 ± 0.12 (Calzolari et al., 2020) increases to 0.47 ± 0.20 with the new calibration. Experimental fault surfaces yielded thin layers of red gouge with localized fault mirror patches comprising sintered nanoparticles (Calzolari et al., 2020). Comparisons of hematite He dates from undeformed, grain-size homogenized hematite with gouge and fault mirror material generated during high velocity slip showed ~13 to 18% and ~35 to 71% He loss, respectively. The He loss from fault mirror patches was interpreted to reflect thermally activated volume diffusion during asperity flash heating (Calzolari et al., 2020). An outstanding question from these high-speed experiments is the extent to which grain size reduction during gouge creation influences He loss.

We thus evaluate the frictional behavior, textures, and potential for He loss from hematite in a new suite of experiments conducted at lower velocity (<1 mm/s) and smaller displacements (<30 mm) than prior work. Such low displacements are similar to observed offsets from many minor hematite slip surfaces in exhumed fault damage zones (DiMonte et al., 2022; McDermott et al., 2017, 2021). Our deformation experiments use the same rotary-shear apparatus and starting material as Calzolari et al. (2020). However, we impose slip rates below 1 mm/s, with the exceptions of an experiment conducted at 10 mm/s over 1.5 m of displacement and an experiment at ~320 mm/s with a displacement of 30 mm. We analyze experimental faults developed within gouge generated from the specular hematite with mechanical data, rate-and-state friction calculations, scanning electron microscopy (SEM), and hematite He thermochronometry. We then compare our observations with prior experiments at seismic slip rates and to natural, hematite-coated faults to characterize coarse-grained hematite frictional and slip behavior.

2. Materials and Methods

2.1. Sample

We utilized the same boulder of coarse-grained, intact specular hematite, collected from the central Wellsville Mountains, Utah, as Calzolari et al. (2020) for deformation experiments to facilitate comparison of our results with their higher velocity experiments, and because this material yields old (U-Th)/He dates that allow us to

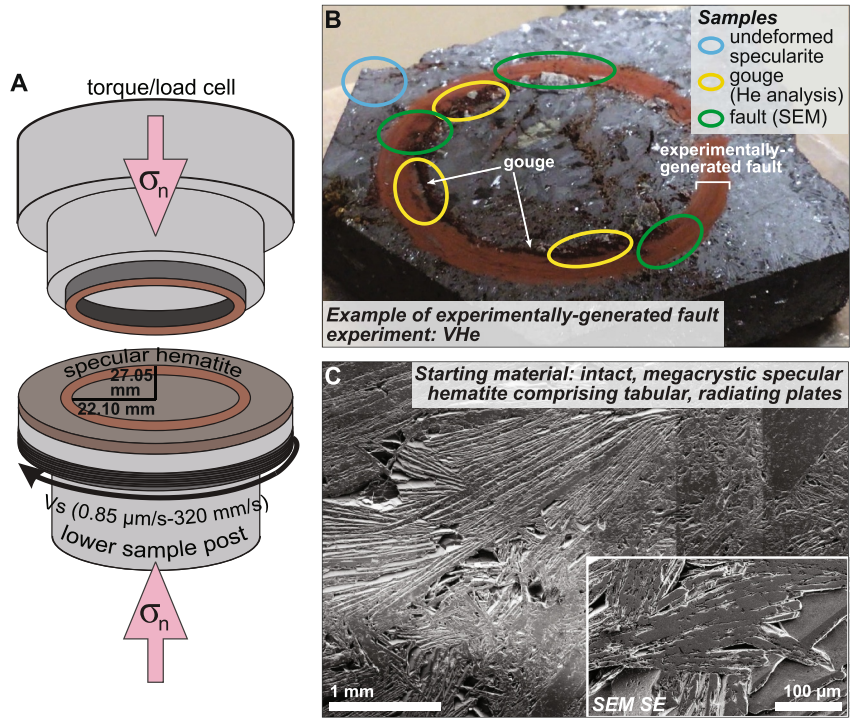

Figure 1. (a) Schematic of the Instron rotary-shear apparatus (modified from Calzolari et al. (2020)). (b) Specular hematite slab from experiment VHe with sampling locations for scanning electron microscopy (SEM) and hematite (U-Th)/He analyses (undeformed starting material, gouge) annotated. (c) SEM secondary electron (SE) images at two scales of coarse-grained starting material.

readily evaluate He loss during deformation experiments. The boulder was cut into ~0.5–1.5 cm slabs with a water-cooled rock saw; the slabs were then epoxied to aluminum plates and gently ground in water to create a flat surface parallel to the aluminum plate, and then roughened with sandpaper. Prior to conducting experiments, the slabs were sonicated for 20 min and dried in an oven at ~100°C for <20 hr (time and temperatures low enough not to induce He loss).

2.2. Rotary-Shear Experiments

Deformation experiments were conducted using the Instron rotary-shear apparatus at Brown University's Rock Deformation Laboratory (Calzolari et al., 2020; Goldsby & Tullis, 2011; Kohli et al., 2011) at ambient room temperature and humidity. The Instron is optimized for experiments on bare rocks surfaces, such as our slabs of intact specular hematite. Frictional deformation was imposed by rotating a cylindrical ring-shaped annulus back and forth against the specularite slab to produce varying amounts of hematite gouge that was further deformed as the experiment progressed (Figure 1). For the annulus, we used Frederick diabase (experiments: S1, V1, V3a, V3b, VHe, SHe01, SHe02, SHe04, SHe05, SHe06), Westerley granite (experiments: V2a, V2b), and SiC (experiment SHe03) (Table 1). These materials were cored to create rings with a ~54.1 mm outer diameter and ~44.2 mm inner diameter (Figure 1a).

Table 1 outlines parameters of each deformation experiment. Experiments were conducted at low normal stresses of 5 MPa (VHe, V3a, V3b) and 8.5 MPa (all other experiments) commensurate with Instron capabilities and to facilitate comparison to the data collected by Calzolari et al. (2020). Experiments involved slip rates primarily from 0.85 µm/s to 1 mm/s, as well as at 10 mm/s and ~320 mm/s. Displacement varied from 10 to 450 mm; for experiments with displacement over ~35 mm, the upper annulus rotated back and forth every 35 mm. Velocity-step tests were carried out on a subset of experiments (V1, V2a, V2b, V3a, V3b, VHe) to characterize velocity-dependent frictional properties. Velocity step-tests began with a velocity of 0.85–10 µm/s (varied with experiment) until a constant coefficient of friction was observed (Table 2). After the initial slip, the controlled sliding

Table 1
Applied Parameters of Friction Experiments

Name	Type	Velocity	Displacement (cm)	Annulus	Load (MPa)	Qualitative assessment of gouge volume
S1	Single-velocity	1 mm/s	~45	Diabase	8.5	Significant
V1	Velocity-step	1–10 mm/s	~45	Diabase	8.5	Significant
V2a,b	Velocity-step	1–500 μm/s	~13, ~26	Granite	8.5	Significant
V3a,b	Velocity-step	10 μm/s-1 mm/s	~10, ~13	Diabase	5	Significant
VHe	Velocity-step	1–100 μm/s	~13.5	Diabase	5	Significant
SHe01	Single-velocity	1 mm/s	1	Diabase	8.5	Minimal
SHe02	Single-velocity	1 mm/s	3	Diabase	8.5	Moderate
SHe03	Single-velocity	1 cm/s	150	SiC	8.5	Significant
SHe04	Single-velocity	0.858 μm/s	1	Diabase	8.5	Moderate
SHe05	Single-velocity	0.858 μm/s	3	Diabase	8.5	Minimal
SHe06	Single-velocity	320 mm/s	3	Diabase	8.5	Moderate

Table 2
Results of a-b From Velocity Step Tests

Name	V_i (μm/s)	V_f (μm/s)	Magnitude of velocity step	μ_f	a-b	Accumulated displacement (mm)
V1_s1	50	1,000	20	0.69	0.0017	10
V1_s2	3	30	10	0.68	0.0065	21
V2a_s1	0.85	50	58.8	0.60	0.002	3
V2b_s1	4	50	12.5	0.68	−0.0088	2
V2b_s2	50	500	10	0.68	−0.0022	9
V3a_s1	10	100	10	0.77	0.0135	3
V3a_s2	100	10	0.1	0.77	0.0012	7
V3a_s3	10	1,000	100	0.78	0.0025	8
V3a_s4	10	1,000	100	0.77	0.0061	36
V3a_s5	10	50	5	0.70	0.0211	71
V3a_s6	50	100	2	0.74	−0.0041	74
V3a_s7	100	500	5	0.75	−0.0035	79
V3b_s1	10	0.85	0.09	0.72	−0.0026	1
V3b_s2	0.85	1,000	1,176	0.75	0.0032	2
V3b_s3	5	500	100	0.74	0.0247	33
V3b_s4	500	50	0.1	0.72	0.0062	52
V3b_s5	50	500	10	0.72	0.0012	54
VHe_s1	10	100	10	0.70	−0.0051	10
VHe_s2	100	1,000	10	0.69	0.0166	43
VHe_s3	100	10	0.1	0.72	0.0029	125
VHe_s4	10	100	10	0.74	0.0072	127
VHe_s5	10	500	50	0.75	0.0026	136
VHe_s6	10	50	5	0.73	−0.0010	174
VHe_s7	50	500	10	0.74	0.0043	185

Note. μ_f is the coefficient of friction at V_f after the velocity step. *s* indicates individual step number.

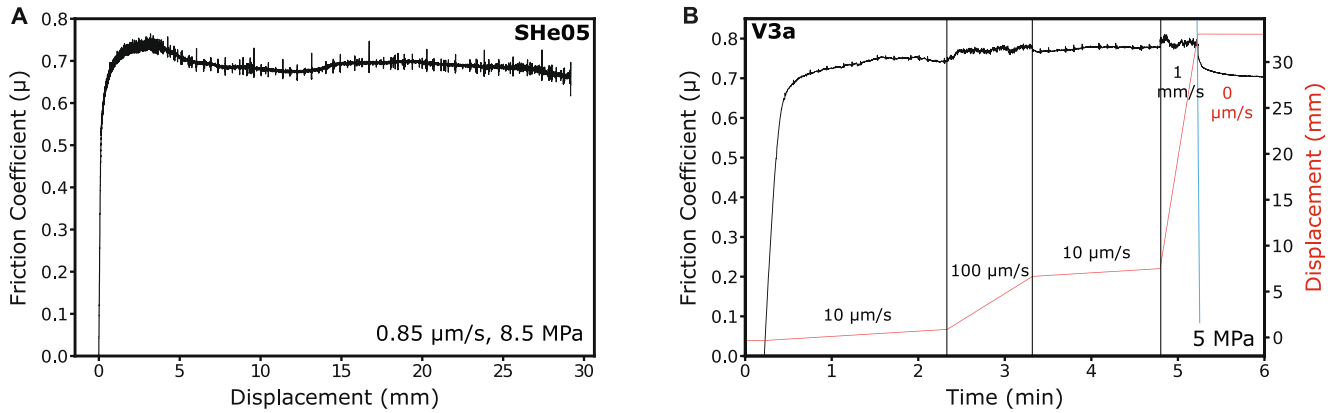

Figure 2. Examples of friction data from single-velocity and velocity-step experiments. (a) Values of coefficient of friction (μ) calculated as a function of displacement for single-velocity experiment SHe05. (b) Values of μ calculated over time for velocity-step experiment V3a.

velocity was stepped up to a new velocity (Table 2, e.g., Figure 2b). Values of the friction rate parameter *a-b* were calculated from Equation 1 (Beeler et al., 1994):

$$a - b = \frac{d(\mu)}{d(\ln(V))} \quad (1)$$

Estimates of the initial and final μ were based on the stabilized μ value immediately prior to a velocity step, and the subsequent steady-state μ observed after the velocity step. Values of $a\text{-}b > 0$ indicate that a material is velocity-strengthening and values of $a\text{-}b < 0$ show that it is velocity-weakening (Beeler et al., 1994; Scholz, 1998).

Data (e.g., torque, load, normal displacement, and angular displacement) were recorded at 20–1,000 Hz sampling rates. Deformation products from single-velocity experiments (S1, SHe01 through SHe06) were analyzed with (U-Th)/He thermochronometry to investigate He loss during deformation. The upper annulus cracked early on during two experiments (V1, V3b) and prior to unloading during several experiments (V2b, VHe, SHe02, SHe03). Such cracks could potentially influence the applied normal stress, although there is no indication that crack formation impacted the data. Experiments conducted at higher slip rates (S1, SHe06) resulted in some slippage of the upper sample grip. This could translate to a lower actual velocity than was prescribed and to a lower bound on the measured torque required for frictional slip. However, the μ values observed during experiments S1 and SHe06 overlap with results from experiments where this slippage did not occur.

2.3. Scanning Electron Microscopy

Secondary electron (SE) and back-scattered electron (BSE) images were acquired using a FEI Quanta FEG 650 scanning electron microscope at Utah State University's Microscopy Core Facility to characterize micro- to nanoscale slip surface textures and to image grains for grain-size measurements essential to the interpretation of hematite He dates. SEM sample mounts were created by cutting small ~3 mm-length blocks using a water-cooled saw. Fault surfaces were epoxied following experiments to preserve textures. Cross-sectional and plan-view sample blocks were isolated from each slab (Figure 1b; Figures S1–S6 in Supporting Information S1) and affixed to ½″ and 1″ metal posts with double-sided, adhesive Cu-tape. Mounts were imaged in low vacuum mode at pressures of 0.15–0.53 torr at 100-100,000x magnification. ImageJ software (Schneider et al., 2012) was utilized to measure the grain size in the samples from images acquired at 1,000–100,000x magnification. We measured the plate-width of tabular grains in the undeformed specularite, the plate-width of tabular grains preserved after deformation, and the diameter of gouge particles generated from the frictional sliding.

2.4. Hematite (U-Th)/He Thermochronometry: Framework and Analytical Approach

Hematite can be analyzed with (U-Th)/He thermochronometry because, during crystallization, it incorporates measurable amounts of U and Th and negligible He, and it retains He over geologic timescales (Bahr et al., 1994;

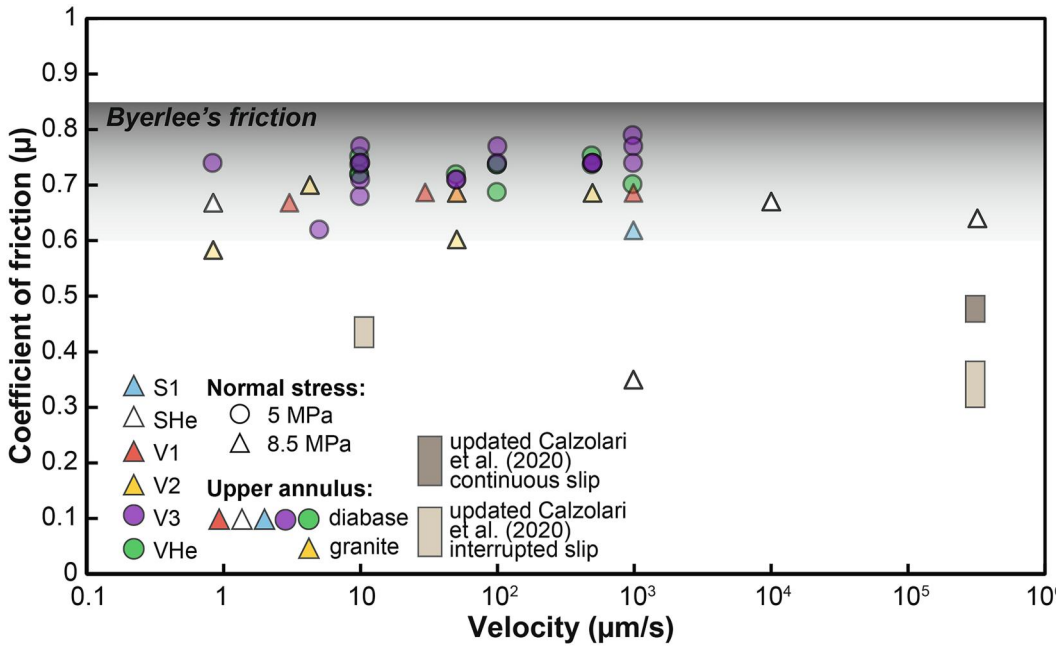

Figure 3. (a) Coefficient of friction (μ) for experiments at velocities of 1 μm/s to 320 mm/s (darker symbols reflect overlapping data points), classified by normal stress (symbol shape) and upper annulus material (color). Recalculated μ of Calzolari et al. (2020) from continuous and interrupted slip experiments for comparison (gray-shaded bars).

Farley & Flowers, 2012; Wernicke & Lippolt, 1993). In natural fault rocks, hematite occurs as polycrystalline aggregates. ^{4}He/^{3}He and ^{4}He diffusion experiments, as well as single crystal (U-Th)/He dates, reveal that individual crystals within these aggregates are the diffusion domain (Evenson et al., 2014; Farley, 2018; Farley & Flowers, 2012; Jensen et al., 2018). Volume diffusion of He through the hematite lattice is a thermally activated process. Because an individual crystal is the diffusion domain, the volume fraction of He loss for a given thermal history decreases with increasing grain size. Thus, the closure temperature (T_c) of the hematite He system, or transition from open to closed system behavior, ranges from ~50 to 250°C and the T_c of a given polycrystalline aliquot is a function of the distribution of grain sizes (i.e., plate thickness of tabular specularite plates, or diameter of cataclastic particles or polygonal grains) (Farley & Flowers, 2012). Each crystal in the aggregate is susceptible to He loss following formation, so the (U-Th)/He date of an aliquot reflects its grain size distribution and associated distribution of T_c. Grain size reduction of hematite during fault slip reduces the diffusion domain length scale, making it subject to He loss at lower temperatures (Ault et al., 2015). "Thermally reset" hematite He dates from fault rocks can reflect He loss due to transient, high temperatures, such as those achieved during seismic slip (Calzolari et al., 2020; McDermott et al., 2017). However, it is unknown if mechanical comminution during fault slip at subseismic rates alone can also induce He loss, as would be expected as a result of exposing He atoms along or near newly formed grain surfaces.

We targeted six single-velocity (SHe01, SHe02, SHe03, SHe04, SHe05, SHe06) experiments and one velocity-step (VHe) experiment for hematite He thermochronometry, comparing results of the undeformed specularite with those from gouge generated during these experiments (Table 1; Figure 1b; Figures S1–S6 in Supporting Information S1). Undeformed material was sampled from the edge of each of the seven hematite slabs, 10s of mms away from the generated fault surface (Figure 1b; Figures S1–S6 in Supporting Information S1). Prior work on this starting material demonstrated a positive relationship between the width of individual plates and single-crystal hematite He dates (Calzolari et al., 2020), reflecting the post-precipitation, long-term thermal history of the rock that induced variable He loss from different-sized plates. To minimize the impact of this grain size effect on hematite He dates from a polycrystalline aliquot, we gently disaggregated starting material from slab edges using a mortar and pestle in ethanol to produce a more homogenous grain size following the approach of Calzolari et al. (2020).

Red gouge material on experimentally generated slip surfaces was removed using a spatula and distributed into aliquots (Figure 1b; Figures S1–S6 in Supporting Information S1). The number of aliquots for each sample was limited by the amount of gouge produced during the experiment. Material was dry pipetted into Nb tubes that were then tightly closed at both ends to prevent loss of powder. Given the fine particle size and delicate nature of the gouge, it was challenging to manipulate this material and deposit it into Nb tubes. Consequently, varying amounts of underlying, undeformed hematite plates were likely incorporated into gouge aliquots.

Aliquots were analyzed for He, U, and Th at the Arizona Radiogenic Helium Dating Laboratory (ARHDL) at the University of Arizona following procedures outlined in Reiners et al. (2014). Details of the analytical methods are described in Text S1 in Supporting Information S1. We do not apply an alpha-ejection correction to our hematite He dates because polycrystalline hematite slabs were created from a larger specimen of pure hematite (e.g., Figures 1b and 1c). Thus, ejection of alpha (He) particles due to their long stopping distances from any given hematite platelet is balanced by alpha-implantation from surrounding material.

3. Results

3.1. Friction Data

The coefficient of friction (μ), measured at velocities of 0.85 μm/s to 320 mm/s ranges from ~0.6 to 0.8 (excluding one outlier), with an average of 0.70 (Figure 3; Table S1 in Supporting Information S1). Reported values are estimated from where the experiment achieved a nominally constant μ during individual velocity steps in the velocity-step experiments (V1, V2a, V2b, V3a, V3b, VHe; Figures S7–S12 in Supporting Information S1) and from single-velocity experiments (S1, SHe01, SHe02, SHe03, SHe04, SHe05, SHe06; Figures S13–S18 in Supporting Information S1). The average μ from the single-velocity experiments is 0.66, excluding the 0.35 outlier. The evolution of μ in each single-velocity experiment varies (Table S1 and Figures S13–S18 in Supporting Information S1).

Calculations of a-b reveal intact specularite exhibits moderately velocity-strengthening to velocity-neutral behavior at slip rates <10 mm/s (Table 2, Figure 4a), with a tendency to become more velocity strengthening at higher velocities (Figure 4b). There is no obvious trend as a function of the magnitude of the velocity step (Figure 4c), although all data form step changes larger than a factor of 10 are positive. The a-b values also appear to become less variable at larger accumulated displacements (Figure 4d). There is a moderately positive trend between the magnitude of the velocity step and a-b and no correlation between a-b and the final velocity in any of the experiments (Figures 4b and 4c).

3.2. Scanning Electron Microscopy

SEM images demonstrate that the starting material comprises undeformed hematite plates with individual plate thicknesses consistent with prior observations (Calzolari et al., 2020) (Figure 1c). Deformation created variable amounts of semi-continuous, unconsolidated gouge and the generated fault surfaces exhibit slickenlines at different scales (Figures 1b and 5). Below and in contact with the gouge layer, hematite plates appear undeformed or display conchoidal fractures where grains are broken (Figures 4a and 4c). Where present, the gouge layer is generally <10 μm thick, but thicker accumulations occur in areas with depressions along the surface of in the starting slab and depressions formed by fracturing of individual plates intersecting the slab surface during slip (Figure 5b). Experiments VHe and SHe03 generated the greatest volume of gouge, with gouge thicknesses in depressions of <100 μm and <60 μm, respectively. Experiments SHe02, SHe04, and SHe06 generated minor volumes of gouge (<50–60 μm-thick in depressions); SHe01 (<30 μm-thick in depression) and SHe05 (<50 μm-thick in depression) did not generate enough gouge to cover the full slip surface. More (i.e., coverage, thickness) gouge was observed after experiments with larger total displacements, however, we do not observe a consistent relationship between μ and the thickness of gouge accumulation (Table 1; Table S1 in Supporting Information S1).

SEM-based grain size analysis of hematite gouge is used to quantify the magnitude of comminution during laboratory deformation (Table S2 in Supporting Information S1). Across all experiments, the diameter of gouge particles ranges from ~0.1 to 65 μm with an average of 0.7 μm. The average particle diameter from each individual experiment ranges from 0.4 to 1.4 μm (Table S2 in Supporting Information S1; Figures 5b and 5d).

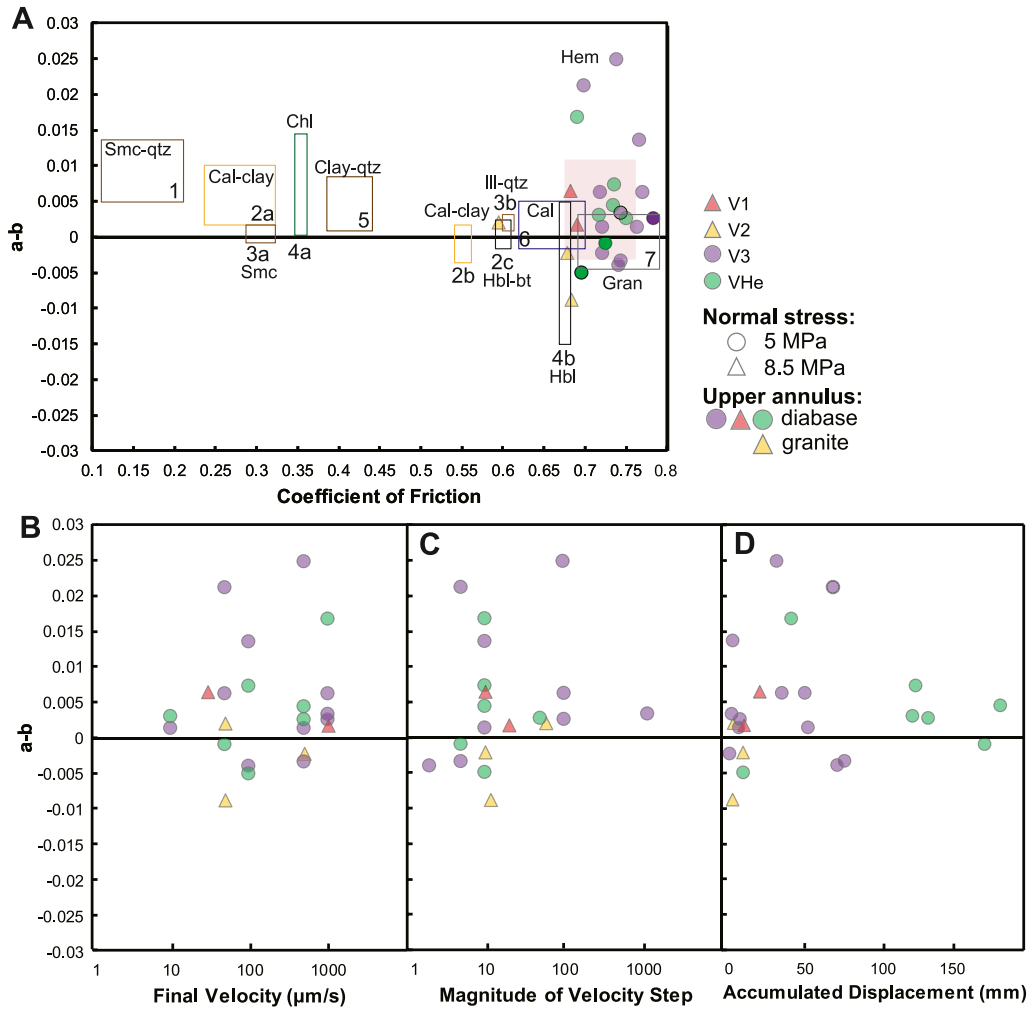

Figure 4. (a) Calculated values of a-b as a function of μ for hematite from velocity step experiments and other mineral assemblages (1—SAFOD (gouge, wet), Carpenter et al., 2012; 2a—Zuccale Cal-trem-clay (foliated rock, room humidity), 2b—Zuccale Cal-trem-clay, (gouge, room humidity), 2c—Zuccale Hbl-bt (gouge, room humidity), Collettini et al., 2011; 3a—Smectite (gouge, room humidity), 3b—Illite shale (gouge, room humidity), Saffer & Marone, 2003; 4a - Chlorite schist (gouge), wet, 4b—Amphibolite (gouge, wet), Fagereng & Ikari, 2020; 5—Opalinus clay (gouge, dry to room humidity), Bigaroni et al., 2023; 6—Calcite/Marble (gouge, wet), Carpenter et al., 2016; 7—Westerley granite (rock, room humidity), Kilgore et al., 1993). Red box is hematite avg ± std. dev; all experiments reported here conducted at 5–15 MPa σ_n. (b) Calculated values of a-b as a function of final velocity for hematite. (c) Calculated values of a-b as a function of the magnitude of velocity step. (c) Calculated values of a-b as a function of the accumulated displacement.

Average gouge particle size decreases toward the slip surface (Figure 5b). Particles are angular to subangular, and some larger particles display conchoidal fractures (Figure 5d).

3.3. Hematite (U-Th)/He Results

We report 49 hematite He dates from (*A*) 27 individual aliquots derived from undeformed, homogenized starting material (3–6 aliquots from each of the slabs used in the seven experiments), and (*B*) 22 individual gouge aliquots (2–5 aliquots from each of six experiments) generated in experiments SHe01, SHe02, SHe03, SHe04, SHe05, SHe06, and VHe (Table S3 in Supporting Information S1). We do not discuss results from gouge from experiment SHe03 owing to Th contamination from the Th-rich SiC upper annulus, which broke down during the deformation experiment and mixed SiC material into the hematite gouge. Analytical uncertainties on individual analyses are ~1–3%, and the standard deviations of all mean sample dates are <10%, with the exception of one sample (SHe02, 11%). In Table 3 we report the mean sample dates ±1σ standard deviation (cf. Flowers et al., 2015) for samples (i.e., replicates of gouge and homogenized starting material from each hematite slab) with three or more

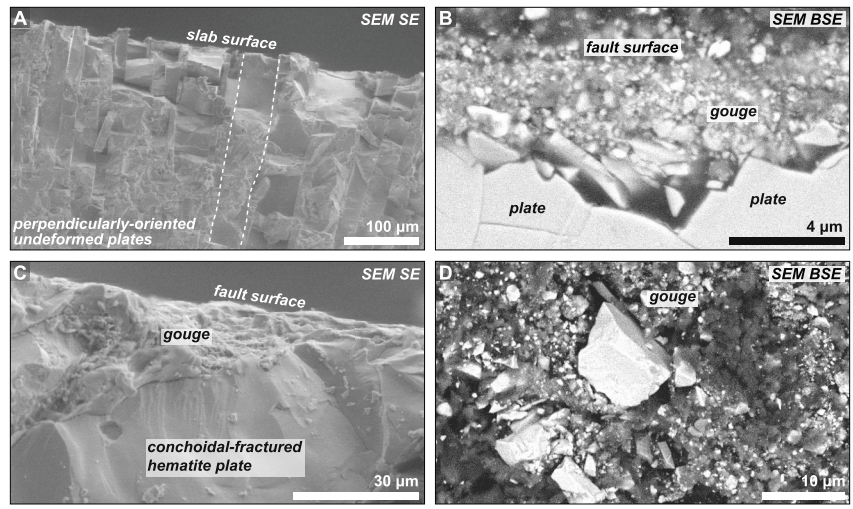

Figure 5. (a) Cross-sectional SEM secondary electron (SE) image of undeformed hematite plates perpendicular to the slab surface. (b) Cross-sectional SEM backscatter electron (BSE) image of depression along slip surface filled with a larger volume of gouge. (c) Cross-sectional SEM SE image of broken hematite plates at the fault surface exhibiting conchoidal fracture with gouge particles in a void. (d) SEM BSE image of gouge particles showing a distribution of grain sizes.

individual analyses and the range of individual analyses for those samples with only two replicates. Individual hematite He dates from all undeformed, homogenized starting material span 236 ± 7 Ma to 155 ± 5 Ma with a mean of 198 ± 17 Ma (9% standard deviation; Figure 6). Individual hematite He dates from gouge range from 206 ± 5 Ma to 136 ± 5 Ma (Table S3 in Supporting Information S1; Figure 6). Details of individual hematite He analyses are reported in Table S3 in Supporting Information S1.

4. Discussion

4.1. Hematite Frictional Behavior

The average μ of 0.7 for coarse-grained, specular hematite is lower than Byerlee's friction at low normal stress ($\mu = 0.85$) commensurate with our experimental conditions, but we note that the variability in our results overlap with scatter in the Bylerlee frictional data (Byerlee, 1978; Figure 3). The sole $\mu = 0.35$ from experiment SHe01 is

Table 3
Hematite (U-Th)/He Date Summary

	Sample	n =	Mean date (Ma)	Std. Dev. (Ma)	% Std. Dev.	Min date ±2σ (Ma)	Max date ±2σ (Ma)
Deformed	SHe1	2[a]				162 ± 5	165 ± 5
	SHe2	5	170	18	11		
	SHe4	2[a]				176 ± 6	193 ± 6
	SHe5	3	202	3	1		
	SHe6	5	153	13	8		
	VHe	5	176	9	5		
Undeformed	SHe1P	4	205	6	3		
	SHe2P	4	188	9	5		
	SHe3P	4	185	11	6		
	SHe4P	4	195	3	2		
	SHe5P	4	187	22	12		
	SHe6P	4	209	10	5		
	VHeP	3	224	8	4		

[a]Where $n = 2$, dates are reported as the minimum and maximum date ±2σ analytical error.

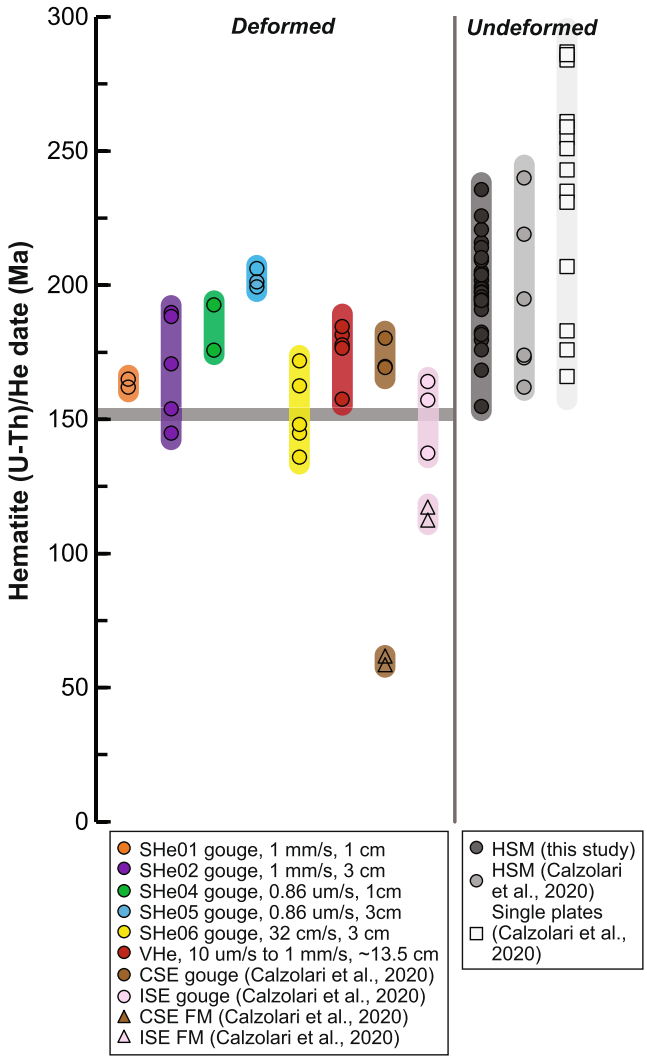

Figure 6. Range of hematite (U-Th)/He (hematite He) dates (individual date $\pm 2\sigma$ analytical uncertainty) of deformed gouge and fault mirror aliquots (colored symbols) from this study and Calzolari et al. (2020) with undeformed (gray symbols, includes homogenized starting material and single plate analyses) aliquots from this study and Calzolari et al. (2020). Horizontal gray bar denotes youngest date (-2σ analytical uncertainty) of the undeformed aliquots across both studies. HSM = homogenized starting material, CSE = continuous slip experiment, ISE = interrupted slip experiment.

considered an outlier. This data point overlaps within error with the recalculated μ of 0.47 ± 0.20 from Calzolari et al. (2020) (Figure 3). The low μ observed at 320 mm/s and over increasing displacement in Calzolari et al. (2020), together with generated fault mirrors and sintered grains, imply dynamic weakening occurred during prior experiments. We do not observe these textures in SHe01 and suggest dynamic weakening did not occur. In addition, there is no relationship between velocity and μ at slip rates from 0.85 μm/s to 10 mm/s (Figure 3), and the type of upper annulus material does not impact the observed range of μ. Experiments also do not yield consistent patterns between μ and gouge thickness or accumulated displacement, indicating that the limited gouge created does not subsequently impact hematite fault strength (Table 1, Figure S19 in Supporting Information S1).

Hematite displays predominantly velocity-strengthening to velocity-neutral behavior at slip rates below ~1 mm/s and, at faster slip rates, it exhibits primarily velocity-strengthening behavior (Figure 4b). The weak increase in a-b at higher magnitude velocity steps (Figure 4c) cannot be explained by an increase in final velocity (Figure 4b). Calculated a-b values commonly decrease with increasing displacement (e.g., Beeler et al., 1996; Ikari et al., 2011; Mair & Marone, 1999; Noël et al., 2023) due to slip localization and fabric development within a gouge layer. Here, we observe scatter in a-b, particularly at low displacements. Development of gouge and slip localization within this gouge may explain the apparent decrease in scatter at higher displacements. However, because the upper annulus rotates back and forth every ~35 mm, preexisting planes of localization are likely destroyed as the slip direction changes and additional gouge is generated. This phenomenon could also contribute to the scatter and observation of primarily velocity-strengthening behavior across all displacements.

For context and comparison, and because limited data exist for hematite relative to other phases, in Figure 4a we highlight the frictional properties of mineral assemblages commonly associated with hematite in fault zones. The friction data were obtained from deformation experiments conducted at room temperature; low normal stress (5–15 MPa); and at dry, wet, or room humidity conditions. The strength and rate-and-state properties of hematite deformed at room temperature and low normal stress are most similar to bare Westerley granite surfaces (Kilgore et al., 1993) and water-saturated calcite (Carpenter et al., 2016). Serpentinite (antigorite) deformed using the same apparatus at similar conditions also displays similar μ and velocity-strengthening behavior at rates <1 mm/s (Kohli et al., 2011). We note that our experiments were conducted at room humidity on rock surfaces that progressively developed gouge. In contrast, most of the comparative experiments were conducted on unconsolidated gouge (except Kilgore et al., 1993, and some experiments from Colletini et al., 2011), and many were deformed at water-saturated conditions (e.g., one experiment from Bigaroni et al. (2023), and experiments from Carpenter et al. (2012, 2016) and Fagereng and Ikari (2020)). For a given material, wet and dry bare surfaces, and wet and dry gouge yield μ values that can differ by 0.4 over a range of normal stresses (e.g., Colletini et al., 2011; Collettini et al., 2009; Mitchell et al., 2016).

Polycrystalline, specular hematite is frictionally strong because its bonds are of a strongly covalent character (Nesse, 2012), and it does not contain weaker van der Waals bonds nor interlayer water like clay minerals (Moore & Lockner, 2004). However, hematite can crystallize as sub-μm-thick, high-aspect ratio platelets analogous to clay minerals, which could promote anisotropic fabric development and subsequent weakening (Collettini et al., 2009, 2011). In contrast, gouge particles generated from specularite during our experiments are angular to subangular, so we would not expect to observe low μ for cataclastic hematite gouge during experiments.

4.2. Textural Development and Comparison to Naturally Deformed Hematite

Hematite gouge in our experiments is produced by brittle fault processes during slip at subseismic rates (Figure 5). The creation of unconsolidated angular to subangular nano- to micro- particles reflects grain-size reduction accomplished by grain fracturing and chipping of rolling grains (Billi, 2010). During slip, elongate plates with an average thickness of ∼17 μm (Figures 1a and 5a; Calzolari et al., 2020) progressively break, dominantly at their tips, to become gouge particles with an average diameter of ∼0.7 μm (0.1, 65 μm, minimum and maximum). Larger gouge particles and broken hematite plates display conchoidal fracture because hematite does not have cleavage. The distribution of gouge particle sizes is similar across all experiments regardless of slip rate and displacement, and the grain size distribution is consistent with observations from Calzolari et al. (2020). However, less gouge is produced during our experiments at lower velocity and lower displacement. In addition, deformation in the higher velocity experiments conducted by Calzolari et al. (2020) also generated localized, mirror-like patches comprising sintered nanoparticles that are not observed in the current study. Despite these differences, we emphasize that in both low- and high-speed experiments, over a range of displacements, brittle deformation of coarse-grained specularite yields unconsolidated gouge.

Experimental cataclasis and gouge production resemble textures formed by brittle deformation in upper-crustal fault zones that developed in coarse-grained specularite veins. In nature, comminution of up to 10s of μm-thick hematite plates that originally crystalize in random to semi-aligned orientations facilitates slip localization and development of thin slip surfaces (Ault et al., 2015, 2019; McDermott et al., 2017, 2023; Odlum et al., 2022). However, in most examples studied to date, gouge particles produced via grain size reduction are subsequently transformed into equant "polygonal" grains with sintered grain boundaries at and below the slip interface (Ault et al., 2015, 2019; McDermott et al., 2017, 2023; Odlum et al., 2022). This transformation reflects transient temperature rise that accompanies seismic slip, but grain size reduction appears to be a pre-requisite of this process.

In contrast to the microstructural evolution of specularite, hematite observed in some shallow fault zones exhibits an anisotropic texture and morphology of high-aspect ratio platelets with an average plate thickness of ∼30 nm and plate length ranging from ∼300 nm to 1 μm (Calzolari et al., 2018; DiMonte et al., 2022; McDermott et al., 2021; Moser et al., 2017). Microstructural analysis of natural samples shows that this foliated, nm-scale hematite does not appear to experience comminution during post-mineralization slip (DiMonte et al., 2022; McDermott et al., 2021). These faults exhibit a scaly fabric and/or S-C-like structures, and deformation is accommodated by sliding between grain boundaries without comminution at subseismic rates (DiMonte et al., 2022). The difference in resulting deformation textures between those generated from μm-scale versus nm-scale hematite implies that initial hematite grain size and textures may influence subsequent deformation processes and, potentially, frictional behavior.

4.3. Assessing the Magnitude and Mechanisms of He Loss During Deformation

Comparison between hematite He dates from undeformed, grain-size homogenized starting material and gouge from experiments SHe01 through SHe06 and VHe allows us to evaluate He loss during low velocity brittle fault slip. (U-Th)/He date is proportional to He content, so we compare hematite He dates from undeformed and gouge aliquots to approximate He loss. Percent He loss was calculated using Equation 2.

$$\%\ \text{He loss} = \frac{\text{Date (undeformed, Ma)} - \text{Date (deformed, Ma)}}{\text{Date (undeformed, Ma)}} \times 100 \quad (2)$$

We conservatively assess the % He loss by comparing average and minimum gouge dates from each experiment to our new and previously published (Calzolari et al., 2020) undeformed starting material dates (Figure 6). Hematite He dates from starting material from each experiment exhibit intrasample scatter (Table S3 in Supporting Information S1, see Figure 1 in Calzolari et al., 2020); we use the full range of undeformed dates across *all experiments* as our benchmark for comparison for several reasons. First, our homogenized starting material aliquots do not have the same grain size distribution and thus hematite He date. Second, the grain size distribution in the starting material is heterogeneous at the scale we sample the slabs and therefore may not reflect the entire range of potential grain-size-dependent dates (cf. Calzolari et al., 2020). In addition, because gouge aliquots may include

larger plates that dominate the He budget (i.e., older dates) by volume, calculated % He loss for each experiment is a minimum estimate.

Across all experiments, most individual hematite He dates from gouge overlap with the younger dates from all undeformed starting material (Table S3 in Supporting Information S1; Figure 6). Experiments SHe06 and SHe02 exhibit He loss (12% and 6%, respectively), when comparing minimum gouge dates to the minimum dates of the entire undeformed data set (Table S4 in Supporting Information S1; Figure 6). Comparison of the average hematite He date of the entire undeformed data set (~197 Ma) to (*A*) the average dates for gouge from each experiment and (*B*) the average date of the entire gouge data set (~172 Ma) indicates that He loss occurred during most experiments. Gouge from the interrupted and continuous slip experiments of Calzolari et al. (2020) exhibit comparable He loss (12% and 22%, Figure 6, Table S4 in Supporting Information S1).

Given the calculated He loss during some experiments, we evaluate the potential role of friction-generated (*A*) average fault surface temperature rise (T_{fs}) and (*B*) asperity flash heating temperature (T_{fh}) along the experimental faults in inducing He loss. We first calculate T_{fs} with Equation 3 (Lachenbruch, 1986):

$$T_{fs} = \frac{\mu\sigma_n}{\rho c} \times \frac{V\sqrt{t}}{\sqrt{\pi\alpha}} \tag{3}$$

where μ (average coefficient of friction from each experiment), σ_n (applied normal stress, 8.5 MPa except for SHe03 at 5 MPa), ρ (hematite density, 5,300 kg/m^3, Nesse, 2012), c (heat capacity, 137.67 J/kgK, Chase, 1983), V (applied velocity for each experiment, m/s), t (experiment time, s), α (thermal diffusivity, 1.55×10^{-5} m2/s, and $\alpha = k/(\rho c)$, where k is thermal conductivity at 11.3 W/mK, Horai, 1971).

We estimate the timescales required to produce the observed He loss in the hematite gouge for the calculated T_{fs} with Equation 4 (Reiners et al., 2007):

$$\ln(t) = \ln\left[\left(\frac{1}{\pi^{\frac{1}{2}}} - \frac{\left(\frac{9}{\pi} - 3f\right)^{\frac{1}{2}}}{3}\right)^2 \frac{a^2}{D_0}\right] + \frac{E_a}{R} * \frac{1}{T} \tag{4}$$

where f (fractional loss), a (radius, cm), D_0 (frequency factor, cm^2/s), E_a (activation energy), R (gas constant, 8.314 J/molK), and T (temperature, K). We assume that the diffusion domain size is defined by a gouge particle radius of 1.2 μm (calculated using the average volume of all particles) and use the hematite diffusion kinetics of Farley (2018) (E_a = 171 kJ/mol, $\ln(D_o) = -0.66$ cm^2/s) (Table S5 in Supporting Information S1).

We focus on experiments SHe06 and SHe02 (Table S5 in Supporting Information S1), which exhibit He loss when comparing the minimum He dates for gouge and undeformed hematite. Calculations reveal that SHe06 generated minor temperature rise of ~107°C (leading to a fault surface temperature of ~127°C). In contrast, the temperature rise for SHe02 is only 6°C (leading to a fault surface temperature of 26°C), which is negligible relative to the ambient room temperature of ~20°C. Based on Equation 4, inducing 12% He loss at 127°C requires a heating duration of ~2 ka. For SHe02, the 6% He loss at 26°C would require a heating duration of ~181 Ga. These calculations indicate an increase in T_{fs} alone does not contribute to He loss within our experimental faults because the duration required to induce He diffusion is obviously well beyond the time over which experiments occurred.

Second, we evaluate if asperity flash heating and associated He loss occurred during experiment SHe06, conducted at approximately seismic slip rates but only 3 cm of displacement. Calzolari et al. (2020) concluded that the substantive He loss (up to 71%) documented at mirror-like patches was due to asperity flash heating during seismic slip at 320 mm/s and 1.5 m of displacement. To evaluate this possibility, we first calculate the temperature required to induce the observed He loss (12%) from a 1.2 μm-radius gouge particle using Equation 4 for an individual asperity. We then calculate the asperity size required to produce T_{fh} with Equation 5 (Archard, 1959):

$$T_{fh} = T_{fs} + \frac{\mu \mathrm{HV}\sqrt{\beta}}{\rho c\sqrt{\pi\alpha}} \tag{5}$$

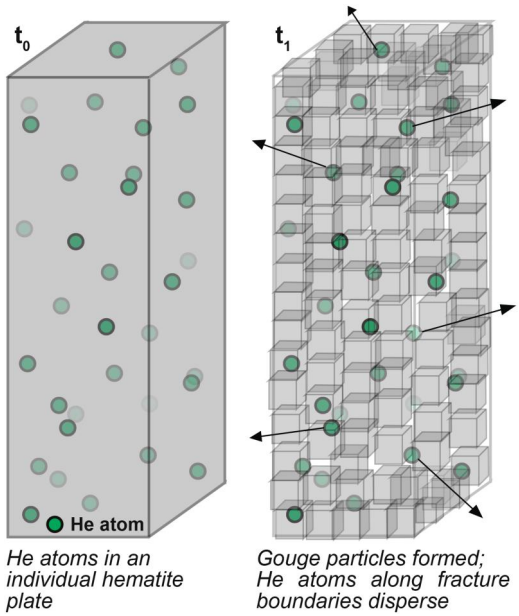

Figure 7. Schematic diagram of a hematite plate with He atoms in but not bonded or charged bound within the crystal lattice (t_0). Hematite plate experiences severe grain size reduction to form smaller gouge particles and He disperses along developed grain boundaries (t_1).

Where (T_{fs}, surface temperature, Equation 3), μ (coefficient of friction), H (indentation hardness, 2.7 GPa, Chicot et al. (2011)), V (velocity, m/s), ρ (density, 5,300 kg/m3), c (heat capacity, 137.67 J/kgK), α (thermal diffusivity, 0.0000155 m^2/s).

Experiment SHe06 would require an asperity diameter of ~7 μm to explain the observed He loss from gouge particles, which is a similar asperity diameter to those suggested by Rice (2006). In comparison, experiment SHe02 would require an asperity diameter >1 mm to explain the observed He loss, which is an unrealistic value. Since asperity flash heating commonly involves only 1%–10% of a slip surface, the associated He loss occurs in a correspondingly small volume of gouge. Thus, the observed He loss in the total volume of gouge analyzed per aliquot in unlikely to have been promoted solely by flash heating. Furthermore, we do not observe textures that nominally accompany flash heating during laboratory slip (cf. Calzolari et al., 2020). In Supporting Information S1, we re-evaluate the diameter of asperities required to explain flash heating-induced He loss in light of the updated coefficient of friction for experiments of Calzolari et al. (2020; see Supporting Information S1).

We suggest He is lost from originally coarse-grained specular hematite solely by intense grain size reduction (Figure 7). Typically, He loss in hematite occurs by thermally activated volume diffusion. The minimum grain dimension (e.g., width of tabular plate or diameter of equant particle) controls the volume fraction of He loss (Balout et al., 2017; Farley, 2018; Jensen et al., 2018) in a given grain and thus aliquot. He loss can also occur via recrystallization (Ault et al., 2015; McDermott et al., 2017); however, we observe no evidence for this process in our experiments. Because we document He loss during our deformation experiments in the absence of a significant calculated fault surface temperature rise or asperity flash heating, we propose that He loss in gouge occurs via comminution alone. In our experiments, gouge generation induces a ~72× increase in surface area of hematite particles, assuming comminution of our average 17 μm-thick and ~2 mm-long plates into cubic gouge particles with a length of ~0.7 μm. Helium is not charged nor bound within the crystal structure (Baxter et al., 2007). Thus, during fault slip, He loss may arise from the formation of extensive new grain surfaces that intersect and expose He where it was previously trapped within interstitial space in the crystal lattice (Figure 7). Density Functional Theory and Kinetic Monte Carlo simulations of He diffusion in goethite and magnetite suggest He is trapped in crystallographic defects and alpha recoil damage (Bassal, Heller, et al., 2022; Bassal, Roques, et al., 2022). If He in hematite is trapped preferentially in recoil damage, we speculate that He loss from gouge could reflect the preferential formation and or propagation of microcracks along damage sites; these microcracks would expose He thereby facilitating He loss during slip and comminution. Grain size reduction may also have contributed to the observed He loss in gouge during the Calzolari et al. (2020) high-speed deformation experiments (Figure 6). Grain size reduction during generation of homogenized starting material was minimal, and the material retained a metallic, specularite appearance, so we infer that notable He loss did not occur during this sample preparation process.

Hematite He dates obtained from natural hematite cataclasite without any textural indications of coseismic friction-generated heat could reflect minor He loss associated with comminution alone. In addition, along hematite fault mirrors where coseismic temperature rise and/or recrystallization are the dominant mechanisms of He loss (e.g., McDermott et al., 2017), a minor portion of the total He loss could be attributed to grain size reduction. The coseismic temperature rise associated with the development of fault mirror surfaces could be overestimated if comminution-assisted He loss is not taken into account. In contrast, nm-scale hematite platelets that deform by sliding along grain boundaries would not be expected to lose He during deformation unless deformation occurred at seismic slip rates. Thus, our experiments support prior inferences that (U-Th)/He dates obtained from small (cm-scale) hematite-coated faults that formed and deformed at transient subseismic slip rates solely reflect the timing of initial mineralization (DiMonte et al., 2022).

5. Conclusions

Our observations reveal that coarse-grained specular hematite is a strong phase that exhibits primarily velocity strengthening to velocity neutral behavior at slip rates of <1 mm/s and displacements <15 cm. This frictional behavior is comparable to deformation experiment results from calcite, granite, and serpentinite experiments conducted at similar conditions (Carpenter et al., 2016; Kilgore et al., 1993; Kohli et al., 2011)—phases and lithologies that are commonly associated with hematite in fault zones. Thin, semi-continuous hematite gouge developed during slip by fracturing and extreme comminution of polycrystalline tabular plates that exposes a greater number of He atoms along many newly formed surfaces. Our comparative hematite He results, together with the lack of fault surface temperature rise or significant asperity flash heating during slip at low velocities, indicate gouge generated during experiments experiences up to ∼10% He loss by a non-thermal process. We suggest that He is lost from hematite along surfaces created during grain size reduction that significantly increases the surface area of the fault material, exposing He atoms along the surface that were previously trapped in the crystal lattice.

Our mechanical, textural and thermochronometric observations have implications for hematite-bearing faults in nature. Hematite faults may accommodate aseismic creep due to its rate-and-state frictional behavior that promotes stable slip at slow driving velocities. Additional experiments are needed to evaluate hematite slip stability at faster velocities, as well as the role of initial grain size and fabric on hematite strength and frictional behavior. Nevertheless, comparisons between our deformation experiments and natural hematite faults highlight that initial grain size and textures may influence subsequent deformation processes and merit additional deformation experiments. Our (U-Th)/He data patterns imply that hematite gouge produced by intense comminution during fault slip may show evidence of He loss solely due to mechanical processes. Fault surfaces characterized by platy, foliated hematite textures with crystals that do not experience grain size reduction during slip should maintain their entire He budget if subsequently deformed at subseismic slip rates. Failure to account for cataclastic grain size reduction may result in an overestimate of coseismic temperature rise from He loss patterns in hematite He thermochronometry data sets.

Data Availability Statement

Information used to derive the interpretations and conclusions of this work are provided in the main text and Supporting Information S1. Relevant data from an in-text data-citation reference, Calzolari et al. (2020, *Geology*) are also included in the Supporting Information S1. The Supporting Information S1 contains text related to methods, Figures S1–19 and Table S1–S6 in Supporting Information S1. The figures and tables in the main text (DiMonte et al., 2024a), Texts S1–S3 and Figures S1–S19 in Supporting Information S1 (DiMonte et al., 2024b), and Jupyter notebooks used to process the data (DiMonte et al., 2024c), are archived and freely available at figshare.com (https://figshare.com/projects/Hematite_frictional_behavior_and_He_loss_from_comminution_during_deformation_experiments_at_slow_slip_rates/190047).

Acknowledgments
This work is supported by U.S. National Science Foundation (EAR-2039727) and Southern California Earthquake Center (SCEC 21068, 22082) grants to Ault and Hirth. This is SCEC contribution no. 13410. SCEC is funded by NSF Cooperative Agreement EAR 1600087 & USGS Cooperative Agreement G17A00047. We thank two anonymous reviewers and Associate Editor Yves Barnabe for detailed and constructive feedback that motivated important organizational and clarifying edits. We thank Pete Reiners, Uttam Chowdhury, and Fen-Ann Shen for analytical assistance and Matt Ikari for helpful conversations and complementary experiments that motivated us to reassess the Instron torque.

References

Allegre, C. J., Poirier, J.-P., Humler, E., & Hofmann, A. W. (1995). The chemical composition of the Earth. *Earth and Planetary Science Letters*, *134*(3–4), 515–526. https://doi.org/10.1016/0012-821x(95)00123-t

Archard, J. (1959). The temperature of rubbing surfaces. *Wear*, *2*(6), 438–455. https://doi.org/10.1016/0043-1648(59)90159-0

Ault, A. K. (2020). Hematite fault rock thermochronometry and textures inform fault zone processes. *Journal of Structural Geology*, *133*, 104002. https://doi.org/10.1016/j.jsg.2020.104002

Ault, A. K., Jensen, J. L., McDermott, R. G., Shen, F.-A., & Van Devener, B. R. (2019). Nanoscale evidence for temperature-induced transient rheology and postseismic fault healing. *Geology*, *47*(12), 1203–1207. https://doi.org/10.1130/G46317.1

Ault, A. K., Reiners, P. W., Evans, J. P., & Thomson, S. N. (2015). Linking hematite (U-Th)/He dating with the microtextural record of seismicity in the Wasatch fault damage zone, Utah, USA. *Geology*, *43*(9), 771–774. https://doi.org/10.1130/g36897.1

Bahr, R., Lippolt, H. J., & Wernicke, R. S. (1994). Temperature-induced ^{4}He degassing of specularite and botryoidal hematite: A ^{4}He retentivity study. *Journal of Geophysical Research*, *99*(B9), 17695–17707. https://doi.org/10.1029/94jb01055

Balout, H., Roques, J., Gautheron, C., Tassan-Got, L., & Mbongo-Djimbi, D. (2017). Helium diffusion in pure hematite (α-Fe2O3) for thermochronometric applications: A theoretical multi-scale study. *Computational and Theoretical Chemistry*, *1099*, 21–28. https://doi.org/10.1016/j.comptc.2016.11.001

Bassal, F., Heller, B., Roques, J., Balout, H., Tassan-Got, L., Allard, T., & Gautheron, C. (2022). Revealing the radiation damage and Al-content impacts on He diffusion in goethite. *Chemical Geology*, *611*, 121118. https://doi.org/10.1016/j.chemgeo.2022.121118

Bassal, F., Roques, J., Corre, M., Brunet, F., Ketcham, R., Schwartz, S., et al. (2022). Role of defects and radiation damage on He diffusion in magnetite: Implication for (U-Th)/He thermochronology. *Minerals*, *12*(5), 590. https://doi.org/10.3390/min12050590

Baxter, E. F., Asimow, P. D., & Farley, K. A. (2007). Grain boundary partitioning of Ar and He. *Geochimica et Cosmochimica Acta*, *71*(2), 434–451. https://doi.org/10.1016/j.gca.2006.09.011

Beeler, N., Tullis, T., Blanpied, M., & Weeks, J. (1996). Frictional behavior of large displacement experimental faults. *Journal of Geophysical Research*, *101*(B4), 8697–8715. https://doi.org/10.1029/96jb00411

Beeler, N., Tullis, T., & Weeks, J. (1994). The roles of time and displacement in the evolution effect in rock friction. *Geophysical Research Letters*, *21*(18), 1987–1990. https://doi.org/10.1029/94gl01599

Behnsen, J., & Faulkner, D. R. (2012). The effect of mineralogy and effective normal stress on frictional strength of sheet silicates. *Journal of Structural Geology*, *42*, 49–61. https://doi.org/10.1016/j.jsg.2012.06.015

Bigaroni, N., Scuderi, M. M., Cappa, F., Guglielmi, Y., Nussbaum, C., Aldega, L., et al. (2023). Frictional properties of Opalinus Clay: Influence of humidity, normal stress and grain size on frictional stability. *Geophysical Journal International*, *233*(1), 211–228. https://doi.org/10.1093/gji/ggac457

Billi, A. (2010). Microtectonics of low-P low-T carbonate fault rocks. *Journal of Structural Geology*, *32*(9), 1392–1402. https://doi.org/10.1016/j.jsg.2009.05.007

Byerlee, J. (1978). Friction of rocks, Rock friction and earthquake prediction (pp. 615–626).

Calzolari, G., Ault, A. K., Hirth, G., & McDermott, R. G. (2020). Hematite (U-Th)/He thermochronometry detects asperity flash heating during laboratory earthquakes. *Geology*, *45*(8), 514–518. https://doi.org/10.1130/G46965.1

Calzolari, G., Rossetti, F., Ault, A. K., Lucci, F., Olivetti, V., & Nozaem, R. (2018). Hematite (U-Th)/He thermochronometry constrains strike-slip faulting on the Kuh-e-Faghan fault, central Iran. *Tectonophysics*, *728–729*, 41–54. https://doi.org/10.1016/j.tecto.2018.01.023

Carpenter, B., Collettini, C., Viti, C., & Cavallo, A. (2016). The influence of normal stress and sliding velocity on the frictional behaviour of calcite at room temperature: Insights from laboratory experiments and microstructural observations. *Geophysical Journal International*, *205*(1), 548–561. https://doi.org/10.1093/gji/ggw038

Carpenter, B., Saffer, D., & Marone, C. (2012). Frictional properties and sliding stability of the San Andreas fault from deep drill core. *Geology*, *40*(8), 759–762. https://doi.org/10.1130/g33007.1

Chase, M. (1983). Heats of transition of the elements. *Bull. Alloy Phase Diagrams*, *4*(1), 124.

Chicot, D., Mendoza, J., Zaoui, A., Louis, G., Lepingle, V., Roudet, F., & Lesage, J. (2011). Mechanical properties of magnetite (Fe3O4), hematite (α-Fe2O3) and goethite (α-FeO· OH) by instrumented indentation and molecular dynamics analysis. *Materials Chemistry and Physics*, *129*(3), 862–870. https://doi.org/10.1016/j.matchemphys.2011.05.056

Collettini, C., Niemeijer, A., Viti, C., & Marone, C. (2009). Fault zone fabric and fault weakness. *Nature*, *462*(7275), 907–910. https://doi.org/10.1038/nature08585

Collettini, C., Niemeijer, A., Viti, C., Smith, S. A., & Marone, C. (2011). Fault structure, frictional properties and mixed-mode fault slip behavior. *Earth and Planetary Science Letters*, *311*(3–4), 316–327. https://doi.org/10.1016/j.epsl.2011.09.020

Cornell, R. M., & Schwertmann, U. (2003). *The iron oxides: Structure, properties, reactions, occurrences and uses*. John Wiley & Sons.

De Paola, N., Holdsworth, R. E., Viti, C., Collettini, C., & Bullock, R. (2015). Can grain size sensitive flow lubricate faults during the initial stages of earthquake propagation? *Earth and Planetary Science Letters*, *431*, 48–58. https://doi.org/10.1016/j.epsl.2015.09.002

Dieterich, J. H. (1979). Modeling of rock friction: 1. Experimental results and constitutive equations. *Journal of Geophysical Research*, *84*(B5), 2161–2168. https://doi.org/10.1029/jb084ib05p02161

DiMonte, A. A., Ault, A. K., Hirth, G., & Bradbury, K. K. (2022). *Hematite accommodates shallow, transient Pleistocene slow slip in the exhumed southern San Andreas fault system*. California.

DiMonte, A. A., Ault, A. K., Hirth, G., & Meyers, C. D. (2024a). Main text figures and tables [Dataset]. *Figshare.com*. https://doi.org/10.6084/m9.figshare.24871356.v1

DiMonte, A. A., Ault, A. K., Hirth, G., & Meyers, C. D. (2024b). Supplemental figures and tables [Dataset]. *Figshare.com*. https://doi.org/10.6084/m9.figshare.24871353.v1

DiMonte, A. A., Ault, A. K., Hirth, G., & Meyers, C. D. (2024c). Jupyter notebook file for processing raw data (.txt files) [Dataset]. *Figshare.com*. https://doi.org/10.6084/m9.figshare.24871332.v1

Di Toro, G., Goldsby, D. L., & Tullis, T. E. (2004). Friction falls toward zero in quartz rocks as slip velocity approaches seismic slip rates. *Nature*, *427*(6973), 436–439. https://doi.org/10.1038/nature02249

Di Toro, G., Han, R., Hirose, T., De Paola, N., Nielsen, S. B., Mizoguchi, K., et al. (2011). Fault lubrication during earthquakes. *Nature*, *471*(7339), 494–498. https://doi.org/10.1038/nature09838

Evenson, N. S., Reiners, P. W., Spencer, J., & Shuster, D. L. (2014). Hematite and Mn oxide (U-Th)/He dates from the Buckskin-Rawhide detachment system, western Arizona: Constraining the timing of mineralization and hematite (U-Th)/He systematics. *American Journal of Science*, *314*(10), 1373–1435. https://doi.org/10.2475/10.2014.01

Fagereng, Å., & Ikari, M. J. (2020). Low-temperature frictional characteristics of chlorite-epidote-amphibole assemblages: Implications for strength and seismic style of retrograde fault zones. *Journal of Geophysical Research: Solid Earth*, *125*(4), e2020JB019487. https://doi.org/10.1029/2020jb019487

Farley, K. A. (2018). Helium diffusion parameters of hematite from a single-diffusion-domain crystal. *Geochimica et Cosmochimica Acta*, *231*, 117–129. https://doi.org/10.1016/j.gca.2018.04.005

Farley, K. A., & Flowers, R. M. (2012). U-Th)/Ne and multidomain (U-Th)/He systematics of a hydrothermal hematite from eastern Grand Canyon. *Earth and Planetary Science Letters*, *359–360*, 131–140. https://doi.org/10.1016/j.epsl.2012.10.010

Flowers, R. M., Farley, K. A., & Ketcham, R. A. (2015). A reporting protocol for thermochronologic modeling illustrated with data from the Grand Canyon. *Earth and Planetary Science Letters*, *432*, 425–435. https://doi.org/10.1016/j.epsl.2015.09.053

Goldsby, D. L., & Tullis, T. E. (2011). Flash heating leads to low frictional strength of crustal rocks at earthquake slip rates. *Science*, *334*(6053), 216–218. https://doi.org/10.1126/science.1207902

Gu, J.-C., Rice, J. R., Ruina, A. L., & Simon, T. T. (1984). Slip motion and stability of a single degree of freedom elastic system with rate and state dependent friction. *Journal of the Mechanics and Physics of Solids*, *32*(3), 167–196. https://doi.org/10.1016/0022-5096(84)90007-3

Horai, K. i. (1971). Thermal conductivity of rock-forming minerals. *Journal of Geophysical Research*, *76*(5), 1278–1308. https://doi.org/10.1029/jb076i005p01278

Ikari, M. J., Marone, C., & Saffer, D. M. (2011). On the relation between fault strength and frictional stability. *Geology*, *39*(1), 83–86. https://doi.org/10.1130/g31416.1

Janecke, S. U., & Evans, J. P. (1988). Feldspar-influenced rock rheologies. *Geology*, *16*(12), 1064–1067. https://doi.org/10.1130/0091-7613(1988)016<1064:firr>2.3.co;2

Jensen, J. L., Reiners, P. W., Siddoway, C. S., Ault, A. K., Thomson, S. N., & Steele-MacInnis, M. (2018). Single-crystal hematite (U-Th)/He dates and fluid inclusions document Cryogenian seismic clastic injection in granite. *Earth and Planetary Science Letters*, *500*, 145–155. https://doi.org/10.1016/j.epsl.2018.08.021

Kaduri, M., Gratier, J. P., Renard, F., Çakir, Z., & Lasserre, C. (2017). The implications of fault zone transformation on aseismic creep: Example of the North Anatolian Fault, Turkey. *Journal of Geophysical Research: Solid Earth*, *122*(6), 4208–4236. https://doi.org/10.1002/2016jb013803

Kilgore, B. D., Blanpied, M. L., & Dieterich, J. H. (1993). Velocity dependent friction of granite over a wide range of conditions. *Geophysical Research Letters*, *20*(10), 903–906. https://doi.org/10.1029/93gl00368

Kohli, A. H., Goldsby, D. L., Hirth, G., & Tullis, T. (2011). Flash weakening of serpentinite at near-seismic slip rates. *Journal of Geophysical Research*, *116*(B3), B03202. https://doi.org/10.1029/2010jb007833

Lachenbruch, A. H. (1986). Simple models for the estimation and measurement of frictional heating by an earthquake. *U.S. Geological Survey Open File Report*, *86–508*, 13.

Leeman, J., Saffer, D., Scuderi, M., & Marone, C. (2016). Laboratory observations of slow earthquakes and the spectrum of tectonic fault slip modes. *Nature Communications*, *7*(1), 1–6. https://doi.org/10.1038/ncomms11104

Mair, K., & Marone, C. (1999). Friction of simulated fault gouge for a wide range of velocities and normal stresses. *Journal of Geophysical Research*, *104*(B12), 28899–28914. https://doi.org/10.1029/1999jb900279

Marone, C. (1998). Laboratory-derived friction laws and their application to seismic faulting. *Annual Review of Earth and Planetary Sciences*, *26*(1), 643–696. https://doi.org/10.1146/annurev.earth.26.1.643

McDermott, R. G., Ault, A. K., & Caine, J. S. (2021). Dating fault damage along the eastern Denali fault zone with hematite (U-Th)/He thermochronometry. *Earth and Planetary Science Letters*, *563*, 116872. https://doi.org/10.1016/j.epsl.2021.116872

McDermott, R. G., Ault, A. K., Evans, J. P., & Reiners, P. W. (2017). Thermochronometric and textural evidence for seismicity via asperity flash heating on exhumed hematite fault mirrors, Wasatch fault zone, UT, USA. *Earth and Planetary Science Letters*, *471*, 85–93. https://doi.org/10.1016/j.epsl.2017.04.020

McDermott, R. G., Ault, A. K., Wetzel, K. F., Evans, J. P., & Shen, F. A. (2023). Microscale spatial variations in coseismic temperature rise on hematite fault mirrors in the Wasatch fault damage zone. *Journal of Geophysical Research: Solid Earth*, *128*(3), e2022JB025069. https://doi.org/10.1029/2022jb025069

Mitchell, E., Fialko, Y., & Brown, K. (2016). Velocity-weakening behavior of Westerly granite at temperature up to 600° C. *Journal of Geophysical Research: Solid Earth*, *121*(9), 6932–6946. https://doi.org/10.1002/2016jb013081

Moore, D. E., & Lockner, D. A. (2004). Crystallographic controls on the frictional behavior of dry and water-saturated sheet structure minerals. *Journal of Geophysical Research*, *109*(B3). https://doi.org/10.1029/2003jb002582

Moore, D. E., Lockner, D. A., & Hickman, S. (2016). Hydrothermal frictional strengths of rock and mineral samples relevant to the creeping section of the San Andreas Fault. *Journal of Structural Geology*, *89*, 153–167. https://doi.org/10.1016/j.jsg.2016.06.005

Morrow, C., Moore, D. E., & Lockner, D. (2000). The effect of mineral bond strength and adsorbed water on fault gouge frictional strength. *Geophysical Research Letters*, *27*(6), 815–818. https://doi.org/10.1029/1999gl008401

Morrow, C., Radney, B., & Byerlee, J. (1992). Frictional strength and the effective pressure law of montmorillonite and lllite clays. In *International Geophysics* (pp. 69–88). Elsevier.

Moser, A. C., Evans, J. P., Ault, A. K., Janecke, S. U., & Bradbury, K. K. (2017). U-Th)/He thermochronometry reveals Pleistocene punctuated deformation and synkinematic hematite mineralization in the Mecca Hills, southernmost San Andreas Fault zone. *Earth and Planetary Science Letters*, *476*, 87–99.

Nesse, W. D. (2012). Introduction to mineralogy.

Noël, C., Giorgetti, C., Scuderi, M., Colletini, C., & Marone, C. (2023). The effect of shear displacement and wear on fault stability: Laboratory constraints. *Journal of Geophysical Research: Solid Earth*, *128*(4), e2022JB026191. https://doi.org/10.1029/2022jb026191

Odlum, M., Ault, A., Channer, M., & Calzolari, G. (2022). Seismicity recorded in hematite fault mirrors in the Rio Grande rift. *Geosphere*, *18*(1), 241–260. https://doi.org/10.1130/ges02426.1

Pozzi, G., De Paola, N., Nielsen, S. B., Holdsworth, R. E., & Bowen, L. (2018). A new interpretation for the nature and significance of mirror-like surfaces in experimental carbonate-hosted seismic faults. *Geology*, *46*(7), 583–586. https://doi.org/10.1130/G40197.1

Reinen, L. A., Weeks, J. D., & Tullis, T. E. (1991). The frictional behavior of serpentinite: Implications for aseismic creep on shallow crustal faults. *Geophysical Research Letters*, *18*(10), 1921–1924. https://doi.org/10.1029/91gl02367

Reiners, P. W., Chan, M. A., & Evenson, N. S. (2014). Radiogenic helium dating and chemistry of diagenetic Fe- and Mn-oxides in Mesozoic sandstones of the Colorado Plateau. *Geological Society of America Bulletin*, *126*(9–10), 1363–1383. https://doi.org/10.1130/B30983.1

Reiners, P. W., Thomson, S. N., McPhillips, D., Donelick, R. A., & Roering, J. J. (2007). Wildfire thermochronology and the fate and transport of apatite in hillslope and fluvial environments. *Journal of Geophysical Research-Earth Surface*, *112*(F4), F04001. https://doi.org/10.1029/2007JF000759

Rice, J. R. (2006). Heating and weakening of faults during earthquake slip. *Journal of Geophysical Research*, *111*(B5), B05311. https://doi.org/10.1029/2005JB004006

Ruina, A. (1983). Slip instability and state variable friction laws. *Journal of Geophysical Research*, *88*(B12), 10359–10370. https://doi.org/10.1029/jb088ib12p10359

Saffer, D. M., & Marone, C. (2003). Comparison of smectite-and illite-rich gouge frictional properties: Application to the updip limit of the seismogenic zone along subduction megathrusts. *Earth and Planetary Science Letters*, *215*(1–2), 219–235. https://doi.org/10.1016/s0012-821x(03)00424-2

Schleicher, A. M., van der Pluijm, B. A., & Warr, L. N. (2010). Nanocoatings of clay and creep of the san Andreas fault at Parkfield, California. *Geology*, *38*(7), 667–670. https://doi.org/10.1130/G31091.1

Schneider, C. A., Rasband, W. S., & Eliceiri, K. W. (2012). NIH image to ImageJ: 25 years of image analysis. *Nature Methods*, *9*(7), 671–675. https://doi.org/10.1038/nmeth.2089

Scholz, C. H. (1998). Earthquakes and friction laws. *Nature*, *391*(6662), 37–42. https://doi.org/10.1038/34097

Scholz, C. H. (2019). *The mechanics of earthquakes and faulting*. Cambridge university press.

Wernicke, R. S., & Lippolt, H. J. (1993). Botryoidal hematite from the Schwarzwald (Germany): Heterogeneous uranium distributions and their bearing on the helium dating method. *Earth and Planetary Science Letters*, *114*(2–3), 287–300. https://doi.org/10.1016/0012-821x(93)90031-4

Williams, R. T., Rowe, C. D., Okamoto, K., Savage, H. M., & Eves, E. (2021). How Fault rocks form and evolve in the shallow San Andreas Fault. *Geochemistry, Geophysics, Geosystems*, *22*(11), e2021GC010092. https://doi.org/10.1029/2021gc010092

Wintsch, R., Christoffersen, R., & Kronenberg, A. (1995). Fluid-rock reaction weakening of fault zones. *Journal of Geophysical Research*, *100*(B7), 13021–13032. https://doi.org/10.1029/94jb02622